AC calorimetry technique. Applications to liquid helium films and liquid crystals

L.M. STEELE[a], G.S. IANNACCHIONE[a,b] AND D. FINOTELLO[a,b]

Department of Physics[a] and Liquid Crystal Institute[b]
Kent State University, Kent Ohio 44242, USA

Recibido el 26 de enero de 1993; aceptado el 15 de abril de 1993

ABSTRACT. We review and detail the use of the AC calorimetry technique as we have applied it to the study of phase transitions. Theory of operation, materials and electronic equipment considerations are discussed in detail. Examples of its use in heat capacity measurements of two-dimensional helium films at sub-Kelvin temperatures and bulk liquid crystal materials at or above room temperature are presented. The high resolution and usefulness of the AC technique are evident from these studies.

RESUMEN. Revisamos y detallamos el uso de la técnica calorimétrica de calentamiento alterno, tal como la hemos aplicado para el estudio de transiciones de fase. Discutimos en detalle la teoría de operación, materiales y equipo electrónico usado. Presentamos ejemplos de su uso en mediciones del calor específico para películas delgadas de helio a temperaturas sub-Kelvin y para cristales líquidos a temperatura ambiente o más altas. La alta resolución y versatilidad de esta técnica son evidentes de estos estudios.

PACS: 07.20.Fw; 65.20+w; 44.60+k

1. INTRODUCTION

Critical phenomena continues to be an extremely rich area of study. In particular, thermodynamic measurements accurately determine critical exponents and hence are of great theoretical interest. The AC calorimetry technique is ideal for the study of phase transitions for several important reasons. Measurements of heat capacity are made at near equilibrium conditions. This is crucial since much of the thermodynamic theory of phase transitions is based on equilibrium considerations. It also allows the use of averaging routines and total automation thus resolving remarkably small heat capacity changes. In most cases, only a small amount of material is required to achieve a high resolution. Finally, strict thermal isolation of the sample from the surroundings (as in an adiabatic technique) is not required. Its implementation is straightforward and adaptable to a variety of physical systems over a wide temperature range.

The versatility of the AC technique is demonstrated by many existing studies on several different systems. Studies of the low temperature properties of superfluid helium films adsorbed in porous glasses [1] and graphite [2], superconducting films [3], melting of nitrogen on graphite [4], bulk liquid crystals [5,9], and free-standing liquid crystal films [10] are a few such examples. It will be further established by the work presented here.

In what follows, we highlight the main features of the AC technique as used in our laboratory. In Sect. 2 we briefly discuss the theory. Experimental details including the electronic equipment used are presented in Sect. 3. Typical data obtained using this technique on low temperature heat capacity studies of helium films adsorbed on anopore membranes is shown in Sect. 4. Also included are heat capacity results obtained from our studies at the second order smectric-A to nematic (AN) and at the weakly first order nematic to isotropic (NI) phase transitions for bulk 8CB liquid crystal. Our data is contrasted to data obtained using another calorimetric method on this same system. A brief summary is presented in Sect. 5.

2. THEORY

2.1 Fundamental principles

The AC calorimetry technique was originally introduced by Sullivan and Seidel [11] in 1968. In this technique, sinusoidal heating by a voltage of frequency f_v is applied to the sample of interest inducing temperature oscillations of frequency $2f_v$. The heat capacity of the sample is inversely proportional to the magnitude of the temperature oscillations. The derivation given below is geometry independent, *i.e.*, the locations of the applied heat and the sensing of the resulting temperature oscillations is unimportant provided certain requirements are met.

A schematic representation of a physical system is shown in Fig. 1. It consists of a heater and thermometer attached, by a thermal conductance K_h and K_θ and having heat capacities C_h and C_θ respectively, to a cell. The sample, of heat capacity C_s, is linked by K_s to the cell. The entire assembly: sample, cell, heater, and thermometer, of total heat capacity C, is linked externally to a regulated thermal bath by a conductance, K_b. A heating voltage, $Q = Q_0(\cos(\omega_v t))^2$, where $\omega_v = 2\pi f_v$ is the angular voltage frequency, is applied through the heater. This induces thermal oscillations of amplitude T_{ac} at an angular frequency, $\omega = 2\omega_v$.

From the solution of the thermal equations of a one-dimensional model for a planar sample with finite conductivity [12], the temperature as measured at the thermometer is given by

$$T_\theta = T_b + \frac{Q_0}{2K_b} + \frac{Q_0}{2\omega C}\left[1 + \frac{1}{(\omega\tau_e)^2} + \omega^2(\tau_\theta^2 + \tau_h^2 + \tau_s^2)\right]^{-\frac{1}{2}} \cos(\omega t - \alpha). \qquad (1)$$

T_b is the bath temperature; the second term is identified as T_{dc}, the sample temperature resulting from the rms heating, while the last term is the induced temperature oscillations. The amplitude of the oscillations can be cast in the form

$$T_{ac} = \frac{Q_0}{2\omega C}\left(1 + \frac{1}{\omega^2\tau_e^2} + \omega^2\tau_i^2\right)^{-\frac{1}{2}}, \qquad (2)$$

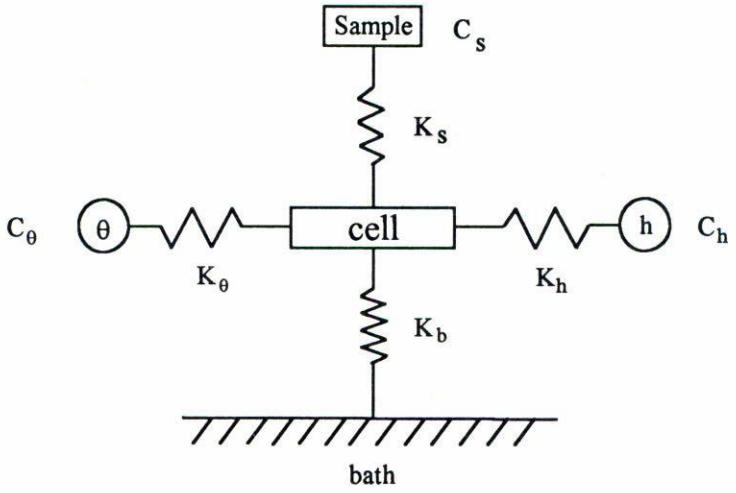

FIGURE 1. The physical system showing the respective thermal links for the sample, thermometer, heater, and bath. The cell is assumed to have a negligibly small internal time constant, *i.e.*, low heat capacity and high thermal conductance, and can be treated as a "short". The addendum heat capacity consists of the cell, heater, thermometer, and adhesives.

with the relaxation times defined by

$$\tau_e = \frac{C}{K_b}, \quad \tau_\theta = \frac{C_\theta}{K_\theta}, \quad \tau_h = \frac{C_h}{K_h}, \quad \text{and} \quad \tau_s = \frac{C_s}{K_s}, \tag{3}$$

where $\tau_i^2 = (\tau_\theta^2 + \tau_h^2 + \tau_s^2)$ is the combined internal time constant of the thermometer (θ), heater (h), and sample (s). It is the time required for the entire assembly to reach equilibrium with the applied heat. The cell is assumed to act like a "short" for the heat, a point of high thermal conductance and low heat capacity; its associated time constant is thus ignored. In the helium work, the cell is a thin brass cup; in the liquid crystal work, a sapphire disk. The external time constant, τ_e, is the time required to reach equilibrium with the regulated bath.

There is also a phase shift between the applied heat and the resulting thermal oscillations, α, and is given by

$$|\tan\alpha| = \left(\frac{1}{\omega\tau_e} - \omega\tau_i'\right)^{-1}, \tag{4}$$

where $\tau_i' = (\tau_\theta + \tau_h + \tau_s)$. The phase shift is related to both the heat capacity and the thermal conductive properties of the entire system. Using Eqs. (3) and (4) and since the external time constant is typically temperature independent and can be measured separately, one can solve for K_s, the sample thermal conductance. If the thermal conductances and heat capacities of the thermometer and heater are small and nearly constant, *i.e.*,

$B = \tau_\theta + \tau_h \cong$ constant, then, K_s may be written as

$$K_s = C_s \left[\left(\frac{1}{\omega^2 \tau_e} - B \right) - \frac{1}{\omega |\tan \alpha|} \right]^{-1}. \tag{5}$$

Hence, in addition to heat capacity measurements, information regarding the thermal conductance may be simultaneously acquired. Ours and other researcher's work [13] indicates that there is a typical phase shift signature associated with the order of the phase transition.

Equation (2) is an exact expression for the total heat capacity. However, by operating at a frequency such that the internal and external time constants do not dominate T_{ac}, an approximation can be made which greatly simplifies the relation between T_{ac} and C. This approximation may lead to a small error in the absolute heat capacity without loss of sensitivity to small changes. If the imposed oscillations are at a frequency "slower" than the sample internal equilibration time but "faster" than the external equilibration time (so that a negligible amount of heat is lost to the bath), then

$$\frac{1}{\tau_e} < \omega < \frac{1}{\tau_i}. \tag{6}$$

Solving for C from Eq. (2)

$$C \cong \frac{Q_0}{2\omega T_{ac}}. \tag{7}$$

The external time constant is controlled by tailoring the thermal link to the bath. It is usually made by thermally anchoring the heater and thermometer electrical leads to a temperature controlled reservoir. This thermal link, on the order of 10 to 100 seconds, is easily adjusted by selecting the appropriate material, length and cross-section for the leads.

Adjustment of the internal time constant is not as straightforward as it strongly depends on the thickness of the sample (the time constants of the thermometer and heater links are again neglected). If the sample thickness is less than the thermal diffusion length given by

$$l = \sqrt{\frac{2K_s A}{\omega C_s}}, \tag{8}$$

where K_s is the sample thermal conductance, C_s its heat capacity and A is the cross-sectional area of the sample, then, the right and side of Eq. (6) is satisfied. Once satisfied, the location of the applied heat and the measurement of temperature becomes unimportant, *i.e.*, the system is now geometry independent. Note that the heat capacity increases linearly while the thermal conductance depends as L^{-1}, with thickness (L). For example, the internal time constant for a sample half as thick, is a factor of 4 shorter.

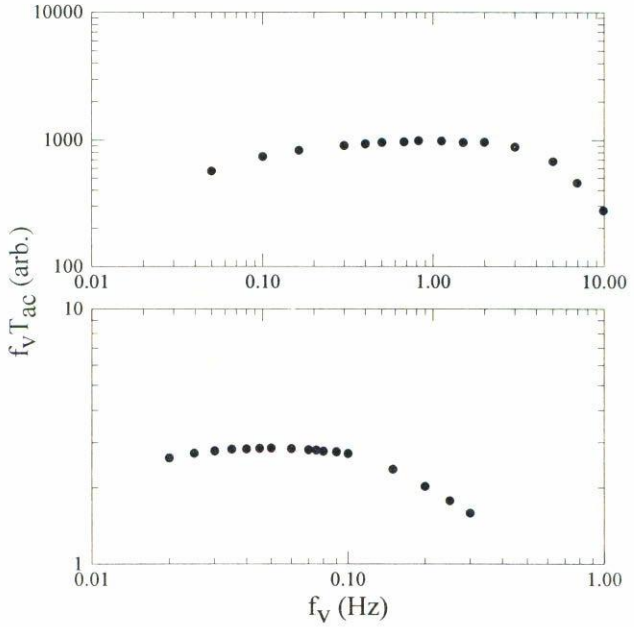

FIGURE 2. Typical frequency scans for the low temperature (above) and the liquid crystal (below) calorimeters.

Experimentally, it is possible to verify if the requirements of Eq. (6) are satisfied by means of a frequency scan. Such a frequency profile is determined by maintaining the same voltage amplitude oscillations at constant temperature while sweeping the frequency and measuring the resulting temperature oscillations. A plot of $f_v T_{ac}$ versus f_v, for a well designed cell, will typically show a "plateau". The plateau indicates the region where the heat capacity will be frequency independent and neither time constant plays a major role (see Fig. 2). The wider the plateau, the smaller the error associated with the use of Eq. (7).

If the amplitude of the applied heat is the peak power dissipated at the heater, $Q_0 = P_p = (V_p)^2/R = P_{pp}/4$, by a voltage V_p applied to a resistance R, then, Eq. (7) can be cast in the form

$$C = \frac{P_{pp}}{32\sqrt{2}\,\pi f_v T_{ac}(\text{rms})}. \tag{9}$$

The addendum heat capacity (cell, thermometer, heater and adhesives) is measured without the sample and subtracted from measurements with the sample present. As in any other heat capacity measurement, the addendum heat capacity should be kept to a minimum in order to maximize sensitivity. This is even more important in the AC technique as a large addendum may lead to a lack of a frequency plateau, or, require an operating frequency too low for lock-in amplification. We close by noting that the AC technique is not suitable to study a first order phase transition because of its oscillatory nature. This is due to the sharp discontinuity in the heat capacity at such a transition. As the system

reaches equilibrium at a new temperature, it spontaneously goes through the transition. At most, a step in the heat capacity might be observed at the transition.

2.2. Thermometry

As evident from Eq. (9), an accurate determination of the temperature oscillations is of primary importance. The oscillations are usually detected with a DC current biased resistor. The absolute temperature is obtained from the calibration of the thermometer, usually as a function of resistance, $T = f(R)$, or, equivalently, due to the DC bias, as a function of voltage. Differentiating, $dT/dR = df(R)/dR = g(R)$, or $dT = g(R)\,dR$. In the limit of small temperature oscillations, $T_{ac} \cong dT$. The temperature about which the sample is oscillating is given by $f(\langle R\rangle)$, where $\langle R\rangle$ is the average resistance of the thermometer. In terms of the voltage drop across the thermometer, $dR = dV/I$, or, $dT = g(V_{dc}/I)V_{ac}/I$, where $dV \cong V_{ac}$ and V_{dc} is the voltage across $\langle R\rangle$, *i.e.*, $V_{dc} = I\langle R\rangle$.

The function $f(R)$ is empirically determined for each sensor used. For carbon flake thermistors, useful in the room temperature work, we have found that

$$\frac{1}{T} = \sum A_n \log(R)^n = A_0 + A_1 \log(R) + A_2 \log(R)^2 + \cdots \tag{10}$$

works rather well. Over the same temperature range, a platinum thermometer can be fit by $T = \sum A_n R^n$. The best fit is chosen as the one with the lowest chi-square with the least number of coefficients, often between 4 and 7.

Speer carbon thermometers, useful at low temperatures, are calibrated against a factory calibrated germanium thermometer as a function of voltage for several different bias currents. This is done to avoid self-heating (Joule's heating) at low temperatures and to maximize the sensitivity at higher temperatures where dR/dT decreases sharply. A carbon resistor is typically fit to $\log(T) = \sum A_n(\log(V))^n$. Since the induced temperature oscillations are obtained from the derivative of the temperature, from Eq. (10),

$$dT \cong T_{ac} = \frac{V_{ac}}{T^2 R_{th} I}\left[A_1 + 2A_2 \log(R_{th}) + 3A_3(\log(R_{th}))^2 + \cdots\right], \tag{11}$$

where $R_{th} = \langle R\rangle$ for the thermistor and T is the temperature is given by Eq. (10). Substituting Eq. (11) in Eq. (9) allows calculation of the heat capacity in terms of measurable quantities:

$$C = \frac{P_{pp} T^2 I R_{th}}{32\sqrt{2}\,\pi f_v}\left[A_1 + 2A_2 \log(R_{th}) + \cdots\right]^{-1}. \tag{12}$$

3. INSTRUMENTATION

A block diagram of the electronic equipment used in our application of the AC calorimetry is shown in Fig. 3. The cell, weakly anchored to a bath regulated at a temperature T_0, has a heater to induce small temperature oscillations on the sample while raising its average

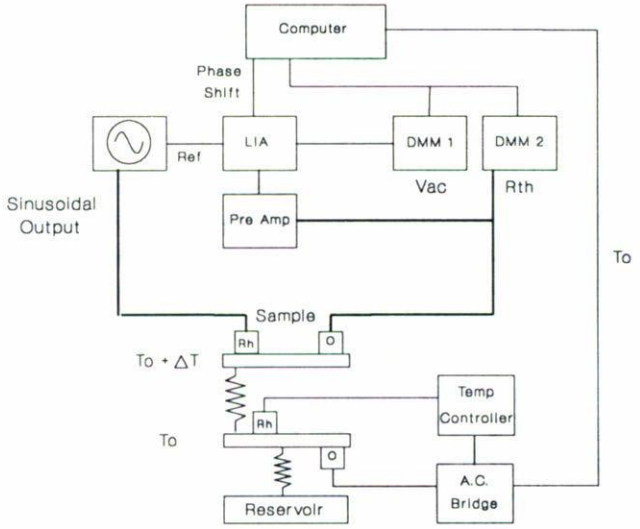

FIGURE 3. Schematic diagram of the instrumentation used for both systems. LIA is a lock-in amplifier, DMM are digital multimeters.

temperature ΔT above the bath. The magnitude of the oscillations is detected by the cell thermometer. Scanning the cell temperature by changing the temperature of the bath, one obtains the heat capacity of the sample as a function of temperature.

Evidently, temperature control is extremely important. In our work, the regulated temperature stability of the bath is better than 100 μK for the liquid crystal work and on the order of a few μK at low temperatures. Resistance thermometry provides the simplest and most convenient measurement and control of temperature. We have achieved the necessary temperature regulation using several resistance bridges/temperature controllers combinations such as the Quantum Design [14] Digital R/G Bridge model 1802, Lakeshore [15] Temperature Controller model DRC-93C, and the Linear Research [16] AC-Resistance Bridge/Temperature Controller models LR-400/LR-130. We have also employed home made AC resistance bridges using a ratio transformer and a lock-in amplifier as the null detector. These provide excellent temperature stability and sensitivity for a variety of sensors, including carbon flake thermistors [17], platinum thermometers [15,18], germanium resistors [15], and ruthenium oxide resistors [18]. These controllers offer different computer control programming features; all of them use Proportional-Integral-Derivative (PID) control action [19], eliminating set point offset, deviation, and overshoot.

The cell thermometer has been measured in two ways, both involving a DC current bias. The first method uses a digital multimeter in resistance mode, naturally applying a constant excitation current to the sensor. Although of excellent current stability, in some cases, it may require an expensive multimeter and the range of available currents if often limited. The second method uses an external current source. The voltage drop across the sensor is read with an inexpensive voltmeter. This allows customization of the applied current. Mercury battery operated current sources have the added advantage of isolation from 60 Hz noise. We have used digital multimeters from Hewlett-Packard [20], Keithley

Inst. [21] and John Fluke Mfg [22]. They are all versatile, reliable and offer convenient computer control programming and interfacing options. Other features include internal noise filtering, signal averaging and 5 to 7 digit accuracy. As mentioned earlier, whether using a multimeter in resistance mode or a current source, care should be take in that no self-heating of the thermometer, causing erroneous absolute temperature readings, occurs. To minimize it, the power dissipated at the cell thermometer is often kept a factor of 100 to 1000 smaller than the power dissipated at the cell heater.

To induce the thermal oscillations we use a wave-form generator operating at the proper frequency (as determined from a frequency scan) and a peak-to-peak voltage for the desired amount of power. Wavetek [23] signal generators have proven to be very stable in amplitude and frequency. The magnitude of the temperature oscillations is dependent on how strong a function of temperature is the sample's heat capacity. Away from a transition, one can afford larger oscillations than near a transition where, due to the rapid heat capacity changes with temperature, rounding will be introduced. Recalling their relation with the temperature derivative, it is however always better to keep them at a minimum.

The signal from the thermometer consists of a DC voltage (often in the millivolt range) mixed with AC oscillations (in the microvolt range). It is read directly and averaged with a multimeter to obtain the absolute temperature ($\langle R \rangle$ or V_{dc}); it is also fed to a pre-amplifier. Here, the DC component is removed while the AC component is amplified and filtered. We use a low noise EG&G 113 pre-amp [24], which provides user adjustable linear amplification with selectable high and low frequency roll offs. The selectable roll offs allow the amplifier bandwidth to be narrowed about the frequency range of interest, increasing the stability of the signal output. The amplified signal is then fed to a low frequency lock-in amplifier operating at 40 or 100 seconds time constant (depending on frequency) for signal averaging. A reference signal for the lock-in amplifier can be provided in one of four ways; splitting the signal generator output driving the cell heater, the signal generator TTL output, a separate signal generator, or the internal oscillator of the lock-in. For the first two methods, the lock-in must operate in 2f mode. The last two methods require the reference to be in phase with the applied power signal, in which case the lock-in operates in 1f mode. We typically use the TTL output of the generator and the 2f mode of operation.

In our studies, we have used an Ithaco 399 [25] and EG&G 5210 dual-phase lock-in amplifiers. The main difference between these models is the limiting low frequency detection. The Ithaco has a low frequency limit of 0.05 Hz as compared to 0.5 Hz for the EG&G. The latter, a digital lock-in amplifier includes GPIB interfacing and offers a wide range of computer controllable parameters. The Ithaco requires an additional coupler to achieve similar computer control. A recently available lock-in amplifier, EG&G 5302, may now be used to frequencies as low as 1 mHz. We note that we have been able to digitize our signals and thus eliminate the need of a lock-in amplifier. However, longer averaging times were required to obtain the same data quality.

The in phase output of the lock-in is averaged with a multimeter (usually and HP 5248) and provides the magnitude of the voltage oscillations, V_{ac}. The out of phase output of the lock-in amplifier is also averaged with a multimeter and it is a measure of the phase shift, α, between the applied and induced oscillations.

The central component of the system is the computer. It is responsible for signal averaging, data storage and automation of the entire system through the GPIB (IEEE-488) standard interface. Specific duties, such as temperature control and voltage of resistance measurements, are left to dedicated devices. After waiting a specified time for the system to come to equilibrium with a new bath temperature, and, allow the lock-in amplifier to stabilize, averaging begins on R_{th} and V_{ac} in blocks equivalent to one or two time constants of the lock-in (usually 125 seconds). A block average is compared to the previous block average and if the difference is within custom specified limits, 0.01 to 0.03%, then, the data taking routine starts. Otherwise, the process of block averaging repeats until stable conditions are achieved. The strictness of the specified limits depends on the long term drifts associated with a particular experimental setup. The data taking routine continues the averaging of R_{th}, V_{ac} and α over a specified number of points. Each point corresponds to one reading of R_{th}, V_{ac} and α. Once completed, the averages are saved to a file, a new bath temperature set and the process begins again. Depending on the application, 3000 data points are averaged after a 5 to 10 minute wait. Data is taken at points 10 mK apart, or less if near a transition. At low temperatures, more closely spaced data can be easily obtained. Given the thermal characteristics, computer speed is unimportant. A 286/12 MHz computer with math co-processor more than satisfies any speed requirements.

Many programming languages allow user defined graphics windows for plotting numerical input. We simultaneously display each device output, monitoring the experiment's progress in numerical and graphical format. Our control program also has an interrupt feature which allows the user to manually operate the experiment.

4. EXPERIMENTAL

4.1. Liquid helium films

The temperature range in this work is 0.05–2 K, achieved with a dilution refrigerator. The calorimeter was constructed as follows. For the cell temperature sensor we used carbon resistors such as Speer™, Allen-Bradley™ and Matsushita™, as well as electrically conducting carbon paint, Electrodag 501 [26-28]. These sensors provide the needed sensitivity and reproducibility as long as they are kept at low temperatures (< 77 K). It is common practice to shave down carbon resistors and remove the bakelite coating to reduce their heat capacity contribution. The power dissipated at the cell thermometers is typically in the nW–pW range. We found that commercially available current sources introduce unwanted ground loops, causing the thermometry to be noisy. Instead, mercury battery powered DC current sources with high resistance metal film resistors were built with switchable is one word current levels in the nA range.

The calorimeter is vacuum tight. The cell consists of inner and outer brass cups, 2.1 cm in diameter and 0.05 mm thick, fitting snugly inside each other. The substrate onto which helium films are adsorbed, Anopore membranes [29], are disks, 60 μm thick with 0.2 μm diameter cavities stacked above one another within the cups. The cell is sealed along the edge with Emerson Cummings [30] 2850 epoxy. Helium is admitted to the cell through a 0.15 mm I.D., 46 cm long coiled cupronickel (or stainless steel) capillary previously

soldered to one face of the cell. The heater is made of 28 Ω/cm Evanohm™ wire, 18 cm long glued with GE varnish [31] to the opposite face of the cell. Its electrical connection is through 0.03 mm diameter copper leads providing an external time constant ranging between 20 and 50 seconds, mostly depending on the heat capacity of the sample. The thermometer, glued with GE varnish to one face of the cell, is a shaved down (0.8 mm thick) Speer carbon resistor with a nominal room temperature resistance of 470 Ω. After shaving, it reads 800 Ω. The Speer thermometer was calibrated against a calibrated Lakeshore Cryotronics germanium resistance thermometer anchored at the platform, using several DC bias currents between 37–495 nA over the temperature range 0.1–2 K. Its electrical connections are two 0.05 mm diameter phosphor bronze leads. Phosphor bronze is used because of its poor thermal conductivity and hence it does not shorten the external time constant. Although the feed capillary, thermometer and heater leads are all thermally anchored to an experimental platform (regulated bath) in the refrigerator, the main thermal link is through the heater leads. The data shown here was obtained with f_v from 0.05 to 2.0 Hz range, μW power dissipated at the cell heater and nA DC bias of the cell thermometer. The induced oscillations ranged between 10 and 1000 μK.

To determine the operating characteristics of the calorimeter, power was applied to the cell. The sample temperature was kept approximately 50 mK above the regulated bath temperature, T_0. By changing frequency, a plateau extending from 0.7 to 5 Hz was found. The frequency scan was repeated at several temperatures bracketing the temperature range of the measurements and an operating frequency chosen. In some cases, usually when a large heat capacity peak was present, two or more frequencies were used. Data taken at different frequencies was overlapped to insure a perfect matching.

Having established the operating frequency, the cell is cooled to the lowest temperature, 0.1 K. Power into the cell is gradually applied until there are measurable thermal oscillations induced in the cell. The temperature of the cell is then changed by gradually increasing the regulated bath platform temperature. As the heat capacity increases and the oscillations amplitude decreases, more power is applied. Again, data taken at different power levels is overlapped. If the amount of helium in the cell was changed to produce a different film thickness, frequency scans were repeated, and as needed, a different operating frequency used.

Prior to adsorbing helium films in the cell, the addendum heat capacity was measured. This is indicated by the solid line in Fig. 4. This configuration has a total addendum heat capacity of 4.5 μJ/K at 0.5 K. Heat capacity data was taken from 0.1 to 2 K and, depending on the features observed, data was spaced every 2–5 mK or 30–50 mK. A selection of heat capacity data for helium films confined in the 0.2 μm cylindrical pores of Anopore membranes are also shown in Fig. 4. Although not fully appreciated from the figure, changes of 1% above the addendum are resolvable given the 0.1% data scatter. The data shown illustrates the high resolution of the technique.

4.2. Liquid crystals

The high temperature calorimeter is designed for versatility and ease of liquid crystal sample placement. A solid brass cylinder is machined such that there is a concentric cylindrical cavity with one open end creating a "ring". The temperature of this ring

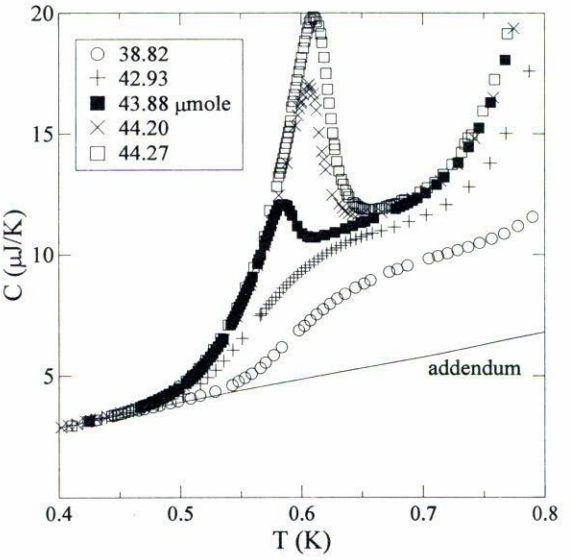

FIGURE 4. **Heat capcity results for several ^{4}He films adsorbed in Anopore membranes. The solid line is addendum heat capacity contribution.**

is the regulated "bath" temperature. Penetrating from the closed end are the electrical connections for the thermometer and the heater. The open end is sealed with a brass cap. A cavity is drilled in the ring wall, parallel to the cylinder axis, and a calibrated, 100 Ω platinum thermometer, is snugly fitted. Wrapped around the exterior of the ring is a resistive (manganin) heater wire. This ring is supported by a 0.3 cm diameter, 4 cm long brass post which provides the thermal link to a larger, evacuated copper chamber. This chamber is rested on a large aluminum block partly submerged in a water bath. With this configuration, we have been able to obtain reliable data over the temperature range between 25 and 125°C. Below room temperatures may be achieved using a TED (thermoelectric device) placed between the copper can and the aluminum block.

The calorimeter consists of a 10 kΩ carbon flake thermistor and a 50 Ω Evanohm heater attached to the same side of a 10 mm diameter, 0.1 mm thick sapphire disk. Sapphire was chosen for its rigidity, flatness, high thermal conductivity, and low heat capacity. It is also compatible with many solvents allowing thorough surface cleaning before sample placement. The thermistor flake has the advantage of its extremely small size, less than 0.05 mm on side, which allows a quick response to temperature changes, *i.e.*, a short internal time constant. Small amounts of adhesive, such as GE varnish or 1266 Stycast [30] epoxy, are used to attach the thermistor and heater to the sapphire disk. This minimizes the addendum heat capacity while ensuring good thermal contact. The temperature sensor, heater, and sapphire disk arrangement has an internal time constant of approximately 1.26 seconds (a high frequency roll off of 0.79 Hz). Attempts with larger thermistors resulted in internal time constants longer than the external time constant, giving an unacceptable frequency profile, *i.e.* no plateau. The heater and thermistor leads are thermally anchored to the ring. The length of the leads from the sapphire disk to the

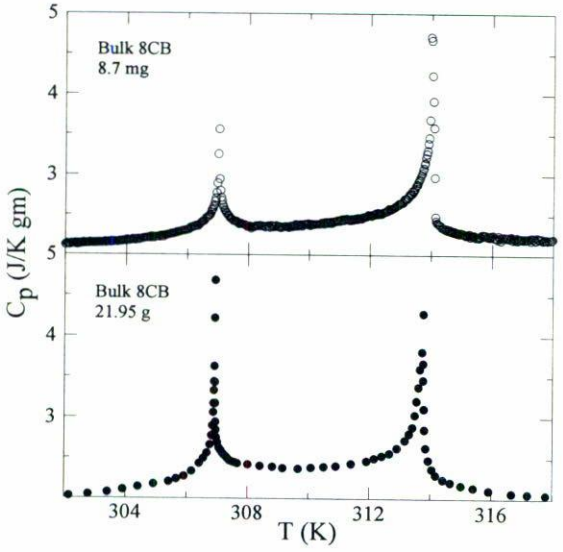

FIGURE 5. Specific heat results for bulk 8CB liquid crystal from this work (top) and that of Ref. [9] (bottom).

ring, and their cross-sectional area, control the external time constant. Here, copper leads, 25 mm long and 0.22 mm in diameter, giving an external time constant of approximately 31.4 seconds (a low frequency roll off of 0.032 Hz) were used. The addendum heat capacity is 42 mJ/K at 30°C. The applied voltage frequency was 0.055 Hz and the induced temperature oscillations were approximately 2 mK in amplitude. With 10 mK steps in temperature, a wait time of 7 minutes and averaging for 8 minutes at each temperature, a relative resolution of 0.2% or better in heat capacity is achieved.

An example of a heat capacity measurement for bulk 8CB, a thermotropic liquid crystal that undergoes a second order smectic-A to nematic and a weakly first order nematic to isotropic phase transition, is shown in Fig. 5. The measurement was performed using less than 9 mg of liquid crystal material forming a droplet and placed on top of the sapphire disk, opposite to the thermistor and heater. It was allowed to spread naturally over the sapphire. We estimate the drop to have a thickness of 0.2 mm over an 8 mm diameter. The system was cycled in temperature several times to ensure complete settling of the material onto the disk. Comparing with Ref. [9], where measurements in a highly sophisticated, high resolution adiabatic scanning calorimeter required 21 grams of material, comparable data quality was obtained with 10^3 less mass. Although we seem to measure a smaller peak at the smectic-A to nematic transition, it is merely a consequence of the large spacing (10 mK) among consecutive data points. After data analysis, identical critical exponents to those quoted in Ref. [9], to within experimental error, were found. This clearly demonstrates the remarkable sensitivity of this technique using very little material. We remark that we have successfully studied liquid crystal phase transitions using less than 2 mg of material [32].

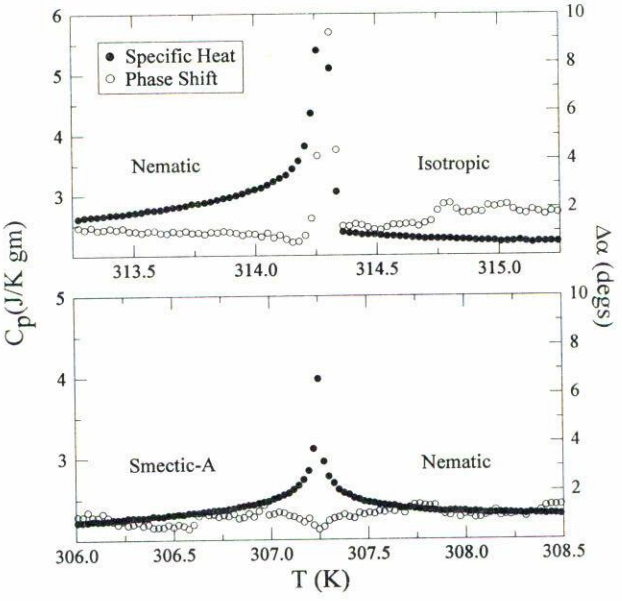

FIGURE 6. The change in phase shift, $\Delta\alpha$, between the applied heat and the induced temperature oscillations and heat capacity for bulk 8CB at the weakly first order, nematic to isotropic, phase transition (above) and the second order, smectic-A to nematic, phase transition (below). For this run, 9.01 mg of 8CB from a different batch was used.

The phase shift change, $\Delta\alpha$, for a different sample of bulk 8CB, 9.01 mg, is presented in Fig. 6. At the weakly first order nematic to isotropic phase transition, there is typically a very sharp peak in $\Delta\alpha$ almost coincident with the observed heat capacity peak. This has been interpreted as being the region of two phase coexistence for a first order transition in the sample. For a second order phase transition there is, typically, a decrease in $\Delta\alpha$, presumably due to the absence of latent heat and a correlation length diverging to macroscopic length scales. For the smectic-A to nematic phase transition of 8CB, we find a very small decrease in the phase shift, consistent with the second order nature of this transition.

5. SUMMARY

We have presented in overview of the AC calorimetry technique and demonstrated its versatility over a wide temperature range. The greatest advantage being its sensitivity at near equilibrium conditions. We have shown that with computer averaging and lock-in amplification detection, high resolution requiring only small samples is achieved. The latter may be important for certain systems where large masses are unavailable. This allows detailed study of many systems and phase transitions. Information on system hardware, computer programming and materials have been referenced whenever possible.

ACKNOWLEDGEMENTS

One of us (D.F.) is grateful to Dr. Roberto Escudero, to the Instituto de Investigaciones en Materiales, UNAM, and to DGAPA, UNAM, for their support and hospitality during the initial stages of this work. This work was supported by NSF Grant DMR 90-13979 and by STC-ALCOM NSF Grant DMR 89-20147.

REFERENCES

1. Y.P. Feng, A. Jin, D. Finotello, K.A. Gillis and M.H.W. Chan, *Phys. Rev.* **B38** (1988) 7041.
2. H.B. Chae and B. Bretz, *J. of Low Temp. Phys.* **76** (1989) 199.
3. T.W. Kenny and P.L. Rickards, *Rev. Sci. Instrum.* **61** (1990) 822.
4. H.K. Kim, Q.M. Zhang and M.H.W. Chan, *Phys. Rev. Lett.* **56** (1986) 1579.
5. J.E. Smaardyk and J.M. Mochel, *Rev. Sci. Instrum.* **49** (1978) 988.
6. C.A. Schantz and D.L. Johnson, *Phys. Rev.* **A17** (1978) 1504.
7. D.L. Johnson, C.F. Hayes, R.J. DeHoff and C.A. Shantz, *Phys. Rev.* **B18** (1978) 4902.
8. J.D. LeGrange and J.M. Mochel, *Phys. Rev.* **A23** (1981) 3215.
9. J. Thoen, H. Marynissen and W. vanDael, *Phys. Rev.* **A26** (1982) 2886.
10. R. Geer, T. Stoebe, T. Pithford and C.C. Huang, *Rev. Sci. Instrum.* **62** (1991) 415.
11. P.F. Sullivan and G. Seidel, *Phys. Rev.* **173** (1968) 679.
12. H.S. Caarslaw and J.C. Jaeger, *Conduction of heat in solids*, Oxford Press (1959).
13. X. Wen, C.W. Garland and M.D. Wand, *Phys. Rev.* **A42** (1990) 6087.
14. Quantum Design, 11578 Sorrento Valley Rd. suite 30, San Diego, CA. USA 92121.
15. Lakeshore Cryotronics Inc. 64 E. Walnut St. Westerville, OH. USA 43081.
16. Linear Research Inc. 5231 Cushman Pl. suite 21, San Diego, CA. USA 92110.
17. Thermometrics Inc. 808 U.S. Highway 1, Edison, NJ. USA 08817.
18. Scientific Instruments Inc. 4400 West Tiffany Dr. Magonia Park, FL. USA 33407.
19. C.L. Nachtigal, *Instrumentation and Control Fundamentals and Applications*, John Wiley & Sons (1990).
20. Hewlett-Packard Co., 5201 Tollview Dr., Rolling Meadows, IL. 60008, USA.
21. Keithley Instruments Inc., 28775 Aurora Rd., Cleveland, OH. 44139 USA.
22. John Fluke Mfg. Co. Inc., PO. Box 9090, Everett, WA. 98206, USA.
23. Wavetek San Diego Inc., 9045 Balboa Ave., San Diego, CA. 92123, USA.
24. EG&G Princeton Applied Research, PO. Box 2565, Princeton, NJ. 08543-2565, USA.
25. Ithaco Inc., 735 West Clinton St. Box 6437, Ithaca, NY. 14851-6437, USA.
26. G.K. White, Experimental Techniques in Low-Temperature Physics, 3rd. ed., Oxford Science (1979).
27. R.C. Richardson and E.N. Smith, *Experimental Techniques in Condensed Matter Physics at Low Temperatures*, Addison-Wesley (1988).
28. O.V. Lounasma, *Experimental Principles and Methods Below 1 K*, Academic Press (1974).
29. Anotec Separations, 226 East 54th St. New York, NY. 10022, USA.
30. Emerson & Cummings, 869 Washington St., Canton, MA. 02021, USA.
31. TRI Research, 2303 Wycliff St., # 2W, St. Paul, MN. 55114, USA. (GE is a registered trademark of General Electric Co.)
32. G.S. Iannacchione and D. Finotello, *Phys. Rev. Lett.* **69** (1992) 2094.